Differential Anomalous X-ray Scattering from an Amorphous Polymer Electrolyte: $[PPO]_xZnBr_2$

James R. Fishburn and Scott W. Barton*

Polymer Science and Engineering Department, University of Massachusetts at Amherst, Amherst, Massachusetts 01003

Received September 23, 1994; Revised Manuscript Received December 12, 1994[⊗]

ABSTRACT: Differential anomalous X-ray scattering (DAS) and extended X-ray absorption fine structure (EXAFS) were used to determine the local structure surrounding the ions in amorphous polymer electrolyte complexes of poly(propylene oxide) and $ZnBr_2$: $[PPO]_6ZnBr_2$ and $[PPO]_{16}ZnBr_2$. On the basis of our results, we propose that $ZnBr_2$ dissociates to form mainly $ZnBr_4^{2-}$ and $Zn(O)_4^{2+}$, where (O) is an ether oxygen on a PPO chain. This observation is contrasted with aqueous $ZnBr_2$, where $ZnBr_2$, $ZnBr_3^-$, and $ZnBr_4^{2-}$ are all observed in the estimated proportions of 2:4:3, respectively. This paper describes the DAS method and its application to structure determination in a multicomponent, amorphous system. In systems with n components, where one or more of the species is a heavy atom, DAS reduces the scattering intensity from a weighted sum of $n(n + 1)/2$ partial structure factors to a sum of partial structure factors which only include the heavy atom of interest.

I. Introduction

Polymer electrolytes are complexes composed of a salt dissolved in a polymer; perhaps the most widely studied examples of this class of materials are the poly(ethylene oxide) (PEO)–salt complexes of the form $[PEO]_nM_mB_b$, where the subscript n denotes the stoichiometric ratio between the moles of PEO mers and moles of added salt, M_mB_b. The solubility of salts such as LiBr, $ZnBr_2$, $NaClO_4$, or their mixtures[1] is driven by the stabilization of a hard Lewis acid cation,[2] such as Li^+, Na^+, Zn^{2+}, etc., by the oxygens on the polyether chain and is further promoted by an anion which is a soft Lewis base such as Br^-, I^-, and ClO_4^-.[2]

The observation, over 20 years ago, that polymer electrolytes are ion conducting[3,4] has since motivated researchers to search for polymer–salt complexes which display sufficient ion conductivity to be used as high energy density batteries and other applications. At this time, however, the conductivity levels are still several orders of magnitude too low to be of practical use. A major obstacle to overcoming the low ion conductivity is a lack of understanding of the conduction mechanism.

The ion conduction is found to occur in the amorphous, rubbery phase of the material[5–8] and often has a temperature dependence which follows the Vogel–Tamman–Fulcher (VTF) equation at temperatures above the glass transition.[7,9,10] Since conductivity does not occur in the crystalline phase of the polymer electrolytes, an ion-channeling mechanism as observed in superionic conductors (β-alumina, AgI) must be ruled out. Furthermore, because of the reported VTF dependence of the conductivity on temperature, the ion mobility is intimately related to the mobility of the polymer chain segments.[10] And while conductivity measurements and theoretical models, such as dynamic percolation,[11] can provide a plausible coarse-grained picture of ion motion in the polymer electrolytes, a complete microscopic interpretation is still absent. We believe that the first step in understanding the dynamics of ion conductivity in polymer electrolytes is to first determine the static structure in the ion-conducting phase.

The important questions that must be addressed are as follows: What are the identities of the ionic species in the system? Where are the ions located with respect to the polymer repeat unit? What is the correlation between mers (the pattern of trans and gauche conformations along the backbone)? The obstacle to structure determination in the amorphous phase is that conventional X-ray or neutron scattering results are uninterpretable since the observed scattering intensity is the weighted sum of at least 10 different partial structure factors!

Extended X-ray absorption fine structure (EXAFS) is one of the few established techniques to probe local order around specific atoms in a condensed matter system.[12] The cation and anion environments in PEO-based polymer electrolytes containing CaI_2,[13] RbBr,[14] ZnI_2,[15] and $ZnBr_2$[15,16] have been studied using EXAFS. In the studies involving CaI_2,[13] a hydrated salt was used and the presence of water made the results difficult to interpret. With the Zn-based polymer electrolytes,[15,16] care was taken to eliminate trace water, and from the EXAFS it was concluded that there was no salt present in the crystalline phase(s); hence information regarding the ions would pertain to the amorphous phase only. The studies revealed that there was significant ion pairing and little dissociation. All the EXAFS results must be regarded with suspicion, as there are serious complications in the determination of reliable coordination numbers.[17,18] Also, EXAFS is limited to probing only the first coordination shell around the atom of interest. This excludes longer range coordinations that are an invaluable aid in structure determination, such as differentiating between square-planar and tetrahedral geometries for an atom with four nearest neighbors.

In this paper, we focus our attention on the problem of the partial structure determination in the amorphous polymer electrolyte $[PPO]_nZnBr_2$, where PPO represents poly(propylene oxide) and n is the number of mers per $ZnBr_2$. We used differential anomalous scattering (DAS) of X-rays with complementary EXAFS to determine the local structure surrounding the Zn and Br in the polymer electrolyte. Used primarily for structure determination in amorphous binary alloys,[19–23] liquids

* To whom correspondence should be addressed.

[⊗] Abstract published in *Advance ACS Abstracts,* February 1, 1995.

0024-9297/95/2228-1903$09.00/0

which contain heavy atoms,[24-27] and concentrated salt solutions,[17,28] DAS is a scattering technique which exploits the change in the atomic scattering factor in the vicinity of an absorption edge.[19] The difference in scattering intensities close to and away from an absorption edge provides the scattering interferences that include only the absorbing species; this considerably reduces the complexity of the total scattering curve. A recent report of X-ray scattering from $[PEO]_nNiBr_2$ electrolytes demonstrates the need for DAS to help specify the local structure.[29] To our knowledge there has been only one other study of polymeric systems with DAS.[30]

PPO was chosen as the host polymer rather than the widely studied PEO to ensure the presence of a single, amorphous phase. In PEO the semicrystalline nature presents an additional complication since one is required to know the percentage of salt that partitions between the crystalline and amorphous phases and one must be able to subsequently separate the amorphous contributions from the scattering intensity;[2,6,31] this difficulty was encountered previously for $[PEO]_nZnBr_2$.[32] The $ZnBr_2$ was chosen because both Zn and Br have absorption edges accessible in the X-ray regime and $ZnBr_2$ is soluble in PPO. While not studied as extensively as complexes with alkali metal salts, there has been some interest in the properties of polymer electrolytes with divalent metal cations.[5,33,34]

We will describe experiments performed on the polymer electrolytes $[PPO]_6ZnBr_2$ and $[PPO]_{16}ZnBr_2$, which we henceforth refer to as the 6:1 and 16:1 samples. Both EXAFS and DAS were used in the determination of local structure surrounding the Zn and Br atoms. While the DAS was used to provide the coordination numbers, the EXAFS was used to identify the atoms in a given coordination shell. In the following sections we will describe the background to DAS (section II), experimental details (section III), data reduction (section IV), and results (section IV) of these experiments. A discussion of the results is presented in section V, where we propose that the $ZnBr_2$ dissociates to mainly the complex ions $ZnBr_4^{2-}$ and $Zn(O)^{2+}$. We draw our conclusions and comment on future work in section VI.

II. DAS Background

A. X-ray Scattering from Heteroatomic Systems. For systems in which there are n different types of atoms, the real space structure is described by a family of $n(n + 1)/2$ different partial pair correlation functions, $g_{ij}(r)$. The Faber–Ziman[35] partial structure factors, $a_{ij}(k)$, are defined in terms of the partial pair correlation function, $g_{ij}(r)$:

$$k[a_{ij}(k) - 1] = 4\pi\varrho_0\int_0^\infty r[g_{ij}(r) - 1]\sin(kr)\,dr \quad (1)$$

where $k = (4\pi/\lambda)\sin\theta$, ϱ_0 is the total average atomic density, and the $g_{ij}(r)$ are defined as the relative probability of finding atoms of type j surrounding the central atom of type i at a specified distance, r. The *partial radial distribution function* (pRDF) follows as

$$\text{pRDF} = 4\pi r^2\varrho_{ij}(r) = 4\pi r^2\varrho_{0j}g_{ij}(r) = 4\pi r^2 c_j\varrho_0 g_{ij}(r) \quad (2)$$

where ϱ_{0j} is the average atomic density of the jth type of atom and c_j is the atomic fraction of the jth type species. The integral over the pRDF from r_1 to r_2 yields the average number of type j atoms in a shell surrounding the central atom of type i. Using this definition for the partial structure factors, the total structure factor, $a_{tot}(k)$, is given by the weighted sum[19-28]

$$[a_{tot}(k) - 1] = \sum_{i=1}^{n}\sum_{j=1}^{n}\frac{c_j f_i f_j^*}{|\langle f\rangle|^2}[a_{ij}(k) - 1] \quad (3)$$

and is related to the normalized, coherent scattering intensity by[19-28]

$$a_{tot}(k) - 1 = \frac{I^{coh}(k) - \langle|f|^2\rangle}{|\langle f\rangle|^2}\ \text{per atom} \quad (4)$$

where

$$\langle|f|^2\rangle = \sum_i c_i|f_i|^2 \quad (5a)$$

$$|\langle f\rangle|^2 = |\sum_i c_i f_i|^2 \quad (5b)$$

From a single X-ray scattering experiment, one can only hope to determine a single, total structure factor. Ideally, one would like to perform $n(n + 1)/2$ unique scattering experiments to extract the individual partial structure factors. In principle, this is possible with X-rays by changing the energy at which the scattering experiment is performed, hence changing the atomic scattering factors $f(k,E)$. In the next subsection we discuss the behavior of $f(k,E)$ as a function of energy.

B. Atomic Scattering Factor. The atomic scattering factor is written as[36]

$$f(k,E) = f_0(k) + f'(E) + if''(E) \quad (6)$$

where f_0 is the energy-independent atomic scattering amplitude; it is the Fourier transform of the isotropic electron density of the atom for which accurate calculated values exist.[37] The second two terms are the anomalous dispersion corrections, which, to an excellent approximation, are independent of k. The imaginary term, f'', is a damping factor proportional to the linear absorption coefficient, $\mu(E)$, by the relation[20]

$$f''(E) = \frac{EM}{4\pi N_A r_e c\varrho\hbar}\mu(E) \quad (7)$$

where E is the energy, M is the atomic mass, N_A is Avogadro's number, r_e is the classical Bohr radius for the electron ($=e^2/(m_e c^2)$), c is the speed of light, and ϱ is the sample density. Examples of f'' may be found in Figure 1a,b, where we plot the anomalous scattering factors for Zn and Br in the vicinity of their respective K shell absorption energies. Note that f'' exhibits EXAFS oscillations at energies above the absorption edge.

The real and imaginary corrections to the atomic scattering factor are related by a Kramers–Kronig transform in the dispersion relation[38]

$$f'(E) = \frac{2}{\pi}\int_0^\infty \frac{E'f''(E')}{E^2 - E'^2}\,dE' \quad (8)$$

Examples of the real correction term are also shown in Figure 1a,b.

Consider the f' and f'' for Zn in Figure 1a. Over an interval within a few hundred eV below the absorption edge, one observes that the real term, f', varies by about 6 electrons and the imaginary term, f'', jumps an

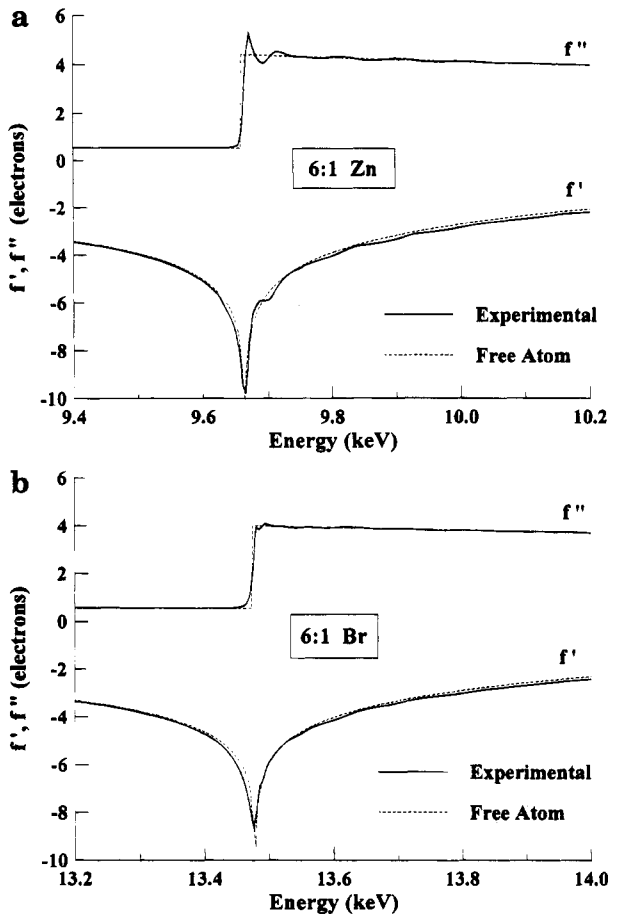

Figure 1. Anomalous scattering factors, $f''(E)$ and $f'(E)$: (a) f'' and f' around the Zn edge of the 6:1 electrolyte; (b) f'' and f' around the Br edge of the 6:1 electrolyte. Solid lines, experimental data; dashed lines, calculated free atom values.

average of 4 electrons at the edge. If one were to perform a series of scattering experiments at $n(n+1)/2$ different energies in the vicinity of the absorption edge, one could separate out the different partial structure factors by varying the scattering strength of the Zn present in the system. This approach has been attempted in systems containing just two types of heteroatoms but is only marginally successful due to the small variations in f' compared to experimental noise.[24] This approach will fail miserably with more than two heteroatoms, as we have in our system. We opt instead for a slightly different anomalous scattering experiment, namely *differential anomalous scattering* (DAS), which we describe next.

C. Differential Anomalous Scattering (DAS). Rather than attempting to determine the individual partial structure factors, a_{ij}, in which both the central atom and the surrounding atom types are specified, we measure the *differential structure factor* (dSF) in which only the type of central atom is specified.

Imagine that we perform two scattering experiments on a heteroatom system using two different energies, E_A and E_B, close to, but below, the absorption edge of one of the components in the system, which we label type 1. For example, let us choose energies at 100 and 5 eV below the K absorption edge to vary $f'(E)$ of atom 1; the scattering amplitude for the other atoms in the system will effectively remain constant over this energy interval. The difference in the scattering intensities is due only to the change in the scattering amplitude of component 1 and thus will contain information about pairwise interactions that *only* include type 1 atoms. We may write the reduced intensity difference as[19-28]

$$\Delta[I^{coh}(k) - \langle|f|^2\rangle] = c_1^2[a_{11}(k) - 1][2\Delta f'_1 \mathrm{Re}(\bar{f}_1) + \Delta(f'_1)^2] + \sum_{j=2}^{n} 2c_1c_j[a_{1j}(k) - 1][\Delta f'_1\,\mathrm{Re}(\bar{f}_j) + \Delta f''_1\,\mathrm{Im}(\bar{f}_j)] \quad (9)$$

where Δ signifies the difference between values at E_A and E_B and $\bar{f}_i$ is the average value of f_i at the two different energies. Note that the structure factors involve only type 1 central atoms. Since we are considering two energies close to each other, but below the absorption edge, where the EXAFS is *not* observed, the term $\Delta f''$ is negligible,[19-28] so eq 9 simplifies to

$$\Delta[I^{coh}(k) - \langle|f|^2\rangle] = 2c_1\Delta f'_1 \sum_{j=1}^{n} c_j\,\mathrm{Re}(\bar{f}_j)[a_{1j}(k) - 1] \quad (10)$$

We may now define a *differential structure factor* (dSF), $a_1(k)$, in analogy to eq 3

$$[a_1(k) - 1] \equiv \sum_{j=1}^{n} \frac{c_j\,\mathrm{Re}(\bar{f}_j)}{\mathrm{Re}(\langle\bar{f}\rangle)}[a_{1j}(k) - 1] \quad (11)$$

which is related to the scattered intensity by eq 10:

$$a_1(k) - 1 = \frac{\Delta[I^{coh}(k) - \langle|f|^2\rangle]}{2c_1\Delta f'_1\,\mathrm{Re}\langle|\bar{f}|\rangle} \quad (12)$$

The *differential radial distribution function* (dRDF) can be related to the partial structure factors by the following expressions:

$$\mathrm{dRDF} \equiv 4\pi r^2\varrho_0 g_1(r) = 4\pi r^2\varrho_0 + \frac{2r}{\pi}\int_0^\infty k[a_1(k) - 1]\sin(kr)\,dk = 4\pi r^2\varrho_0 + \frac{2r}{\pi}\sum_{j=1}^{n} c_j\left[\int_0^\infty \frac{\mathrm{Re}(\bar{f}_j)}{\mathrm{Re}\langle\bar{f}\rangle}\sin(kr)\,dk\right]\otimes\left[\int_0^\infty k[a_{1j}(k) - 1]\sin(kr)\,dk\right] \quad (13)$$

where $\otimes$ represents a convolution. If it is known that *only* type j atoms occupy a coordination shell between r_1 and r_2, then the coordination number of type j atoms which surround the central type 1 atom is given approximately by

$$N_{1j} \approx \left\langle\frac{\mathrm{Re}\langle\bar{f}\rangle}{\mathrm{Re}\,f_j}\right\rangle_{k_p}\int_{r_1}^{r_2}[4\pi r^2\varrho_0 g_1(r)]\,dr \quad (14)$$

where the quantity in brackets $\langle\ldots\rangle$ is evaluated at $k_p = 2\pi/r_p$, where r_p is the distance at the peak of interest in the dRDF.[39]

III. Experimental Procedures

A. Sample Preparation. The PPO (Aldrich, MW = 4000, hydroxyl terminated) and anhydrous zinc bromide (99.999%, Aldrich) were used as received. To prevent air or moisture contamination, all steps of sample preparation were performed under a dry N_2 atmosphere, either in a glovebox or in a desiccator over molecular sieves.

Table 1. Comparison of Coordination Parameters of $ZnBr_2$ in Various Solvents from This Work and from Others[a]

source	this work	this work	this work	this work	ref 16	ref 15	ref 17	ref 52	ref 58	ref 15
solvent	(PPO)	(PPO)	(PPO)	(PPO)	(PEO)	(PEO)	(H_2O)	(H_2O)	(H_2O)	none
technique	DAS	EXAFS	DAS	EXAFS	EXAFS	EXAFS	DAS/EXAFS	X-ray scat	EXAFS	X-ray scat
conc	6:1	6:1	16:1	16:1	8:1	12:1	8.08 M	2.51 M	3.23 M	
Zn										
r_{Zn-Br} (Å)	2.39	2.30	2.39	2.32	2.34	2.339	2.37	2.365	2.37	2.41
r_{Zn-O} (Å)	2.13	2.00	1.98	2.00	2.23	2.230	1.95		1.94	
n_{Zn-Br}	1.4–1.8	0.955[b]	3–4	0.998[b]	1.80	2.1	2.4	1.34	3.00	4
n_{Zn-O}	1.9–2.3	0.874[b]	2–4	1.324[b]	4.61	6.4	1.2		4.50	
Br										
r_{Br-Zn} (Å)	2.39	2.30		2.37		2.334	2.38	2.365	2.37	2.40
r_{Br-Br} (Å)	4.05	3.97					3.99	4.000		~4.00
n_{Br-Zn}	0.9–1.2	0.960[b]		1.010[b]		0.8	1.2	0.67	1.50	2
n_{Br-Br}	4.8–5.2	1.126[b]					4–6	0.5		12

[a] The final column represents data from crystalline, anhydrous $ZnBr_2$. [b] The coordination numbers from the EXAFS are not reliable estimates. A total coordination number of $n_{Zn-Br} + n_{Zn-O} = 3.7$ was consistently determined.

The samples were prepared by dissolving stoichiometric amounts of PPO and $ZnBr_2$ in a minimum of methanol. The methanol (Aldrich, HPLC grade) was dried by distillation over Mg and I_2.[40] After stirring for ~48 h, the solutions were transferred to a desiccator which was purged with dry N_2 for 48–72 h at room temperature. The polymer electrolytes were then held under vacuum, first for 48 h at room temperature and then for 24 h at 75 °C. This ensured the removal of residual methanol. After drying, the samples were stored in the drybox. The same batches were used for the scattering and absorption studies.

When salt was added to the PPO, an increased viscosity was observed, but the samples remained in the liquid state. DSC was used to measure glass transitions for PPO, the 16:1 sample, and the 6:1 sample at −61.6, −47.7, and −13.3 °C, respectively.

B. EXAFS. Standard transmission EXAFS experiments were performed at the Zn and Br K shell edges (9.659 and 13.474 keV, respectively) by monitoring the beam intensity with gas-filled ionization chambers before and after the sample transmission.[12]

C. X-ray Scattering. The scattering experiments were performed on the D-1 line at the Cornell High Energy Synchrotron Source (CHESS) using a diffractometer which was constructed by us utilizing a symmetric $\theta-2\theta$ reflection geometry. A double-bounce Ge(111) monochromator selected the desired energy with a resolution of 4.9 eV at 9.6 keV and 8.5 eV at 13.4 keV. To detect the scattered radiation, we used a Si(Li) energy-dispersive detector, which was required to separate the elastically scattered radiation from the X-ray Raman scattering[41,42] and fluorescence.[21] The amplified output from the detector was fed into a multichannel analyzer (MCA). A 70 Hz precision pulser was also passed into the MCA through the detector amplification circuit to make dead time corrections at high count rates. The data collection and $\theta-2\theta$ motion were controlled by a personal computer.

The sample holders were made from liquid cells originally intended for X-ray fluorescence (SPEX, Model 3516). The cell consisted of a polypropylene tube with a 31 mm inside diameter. A 3 μm Mylar window covered one end of the tube while the other end was sealed with a PTFE base plug which had a tapped hole in the center used to allow spillover when the plug was put into place. The samples were loaded and sealed into the cells inside a dry N_2 glovebox.

For the Zn DAS experiments, the scattering energies were 3 and 97 eV below the Zn absorption edge for both the 6:1 and 16:1 samples. For the 6:1 sample, the Br DAS experiments were performed at 12 and 102 eV below the Br edge, while the energies were 6 and 102 eV below the Br edge for the 16:1 sample. At the Zn edge energies a spectrum was recorded every 0.025 $Å^{-1}$ in a range of $k = 0.200-8.000$ $Å^{-1}$. At the Br edge a spectrum was recorded every 0.035 $Å^{-1}$ from $k = 0.300$ to $k = 12.000$ $Å^{-1}$. We sacrificed statistical accuracy for speed by recording a spectrum at each angle for only 1 min.

IV. Data Reduction

A. EXAFS. The absorption data were analyzed by standard procedures[12] using a commercial software package, BAN (Tolmar Instruments, Hamilton, ON), and the results of the analysis for the 6:1 and 16:1 samples are presented in Table 1.

B. Anomalous Scattering Factors. We calculated f' and f'' using our experimental absorption measurements and eqs 7 and 8.

The imaginary anomalous correction term, f'', was calculated from the experimentally measured absorption coefficient, $\mu(E)$, using the atom-specific version of eq 7:

$$f''_i(E) = \frac{E_0 M}{4\pi N r_e c \varrho_j \hbar} \mu_i(E) \qquad (15)$$

where i is Zn or Br. To obtain μ_i from the measured, total absorption coefficient, μ_{tot}, the experimental curve was scaled to the edge jump calculated from the standard absorption tables.[43] The μ_j's were then subtracted from the normalized μ_{tot}, and any remaining curvature in the resulting μ_i was removed by spline fitting. In this and all subsequent analysis, we assumed a zero volume change upon mixing, so that the partial densities in the complex were $\varrho_i = c_i \varrho_{0i}$, where c_i is the atomic fraction and ϱ_{0i} is the partial density in the pure component (polymer or electrolyte). The $f''(E)$ values for the Zn and Br in the 6:1 samples are shown in Figure 1.

The $f'(E)$'s were determined for both Zn and Br from $f''(E)$ using the integral dispersion relation[38] in eq 8, which was integrated using the procedure of Hoyt et al.,[44] and these are shown in Figure 1 for the 6:1 sample. For comparison, the free-atom values are shown and one can clearly see the differences in the vicinity of the absorption edge.

C. DAS. Several corrections were necessary to convert the observed intensity to the absolute coherent intensity, $I^{abs}(k)$, namely (1) stripping the X-ray resonance Raman intensity, (2) correction for detector dead

time and incident beam intensity fluctuations, (3) subtraction of the scattering from an empty sample cell, and (4) normalization with removal of the incoherent and multiple scattering.

The Kβ resonant Raman and Compton (incoherent) scattering were not resolved from the elastic scattering with the Si(Li) detector. We calculated the intensity of the Kβ component from the observed Kα intensity and the relative fluorescence rates for the Kα and Kβ lines, with corrections made for absorption at the two different energies.[26,45] The calculated Kβ intensity was then subtracted from the integrated intensity at the elastic peak position for each energy spectrum.

At each wavevector, the detector dead time was corrected by dividing the elastic peak intensity by the integrated pulser intensity, and the incident beam fluctuations were corrected to the total intensity measured on an incident beam ionization detector located upstream of the sample. The background radiation was measured before each run with an empty cell and was subtracted from the intensity values at the elastic scattering energy. Next, the standard absorption,[46] normalization,[46-48] and multiple scattering[49] corrections were made, using tabulated values for the atomic incoherent scattering,[50] to produce the coherent scattering intensity, $I^{coh}(k)$.

The difference intensity used in section II.C was expressed as

$$\Delta[I^{coh}(k) - \langle|f|^2\rangle] = I^{abs}(k,E_A) - I^{abs}(k,E_B) \quad (16)$$

and used to calculate the differential structure factor (dSF) in eq 12. The total and differential structure factors for the 6:1 and 16:1 samples are shown in Figure 2.

The dSFs were finally transformed via a modification of eq 13 into the reduced differential radial distribution function (rdRDF)[17]

$$r[\varrho(r) - \varrho_0] = \frac{1}{2\pi^2}\int_0^\infty k[a_1(k) - 1]\, M(k) \sin(kr)\, dk \quad (17)$$

and these are shown in Figures 3a and 3b. A relatively large value of $\sigma = 0.030$ was used in the convergence factor, $M(k)$ (=exp($-\sigma k^2$)), to damp out the spurious peaks due to truncation effects.[51]

D. DAS Results. In Figure 3a, the only prominent feature in the 6:1 Zn edge rdRDF is the large peak at ~2.3 Å; from the EXAFS analysis, we determined that both Zn–O and Zn–Br coordinations contributed to this correlation. As expected, a peak at the same distance is observed in the 6:1 Br edge rdRDF, which the EXAFS results indicated was a Br–Zn coordination. Two other peaks at ~4.00 and ~8.00 Å are also prominent in the 6:1 Br edge rdRDF. Based on our EXAFS analysis and other studies,[17,52] the peak at 4.00 Å is assigned to Br–Br coordination. The 8.00 Å peak is not assigned but could be due to additional Br–Br correlations.

As in the 6:1 sample, the 16:1 rdRDF (Figure 3b) shows one prominent peak in the Zn edge rdRDF, at ~2.3 Å, and based on the EXAFS analysis, both Zn–O and Zn–Br coordinations contributed to this peak. In the 16:1 Br edge rdRDF the Br–Zn coordination peak is present at ~2.3 Å. There also appears to be a peak at 3.5 Å.

The coordination numbers for the different atom–atom pairs are obtained from the dRDFs (eq 13), shown in Figure 4a–d. The coordination numbers were determined from fitted Gaussian peak areas in the dRDFs and by using the approximation in eq 14. All the nearest neighbor distances and estimated ranges of coordination numbers are presented in Table 1 along with the results obtained from the EXAFS analysis. In addition, the results from other related studies are presented for comparison. The width of the peaks in the dRDFs varied slightly with the damping factor σ in eq 17; however, with any reasonable variation of σ, the areas remained similar for the peaks in both the Zn and Br dRDFs.

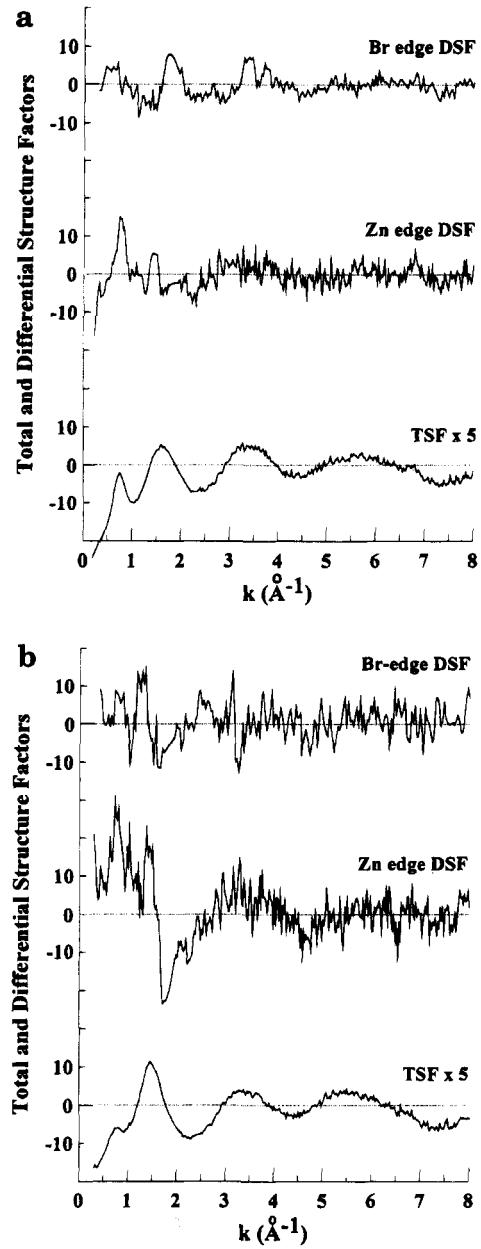

Figure 2. Total and differential structure factors: (a) 6:1 sample; (b) 16:1 sample. In both (a) and (b) the total structure factor is scaled by a factor of 5.

V. Discussion

A. $[PPO]_6ZnBr_2$ (6:1). In the 6:1 sample we found that, on average, each Zn^{2+} shell is coordinated with ~1.8 Br^- anions and ~1.9 oxygens. With the cumulative errors of the truncation effects in the transform and the fitting of the peak in the dRDF, we interpret the total coordination $n_{Zn-Br} + n_{Zn-O}$ as 4. Because Zn^{2+}

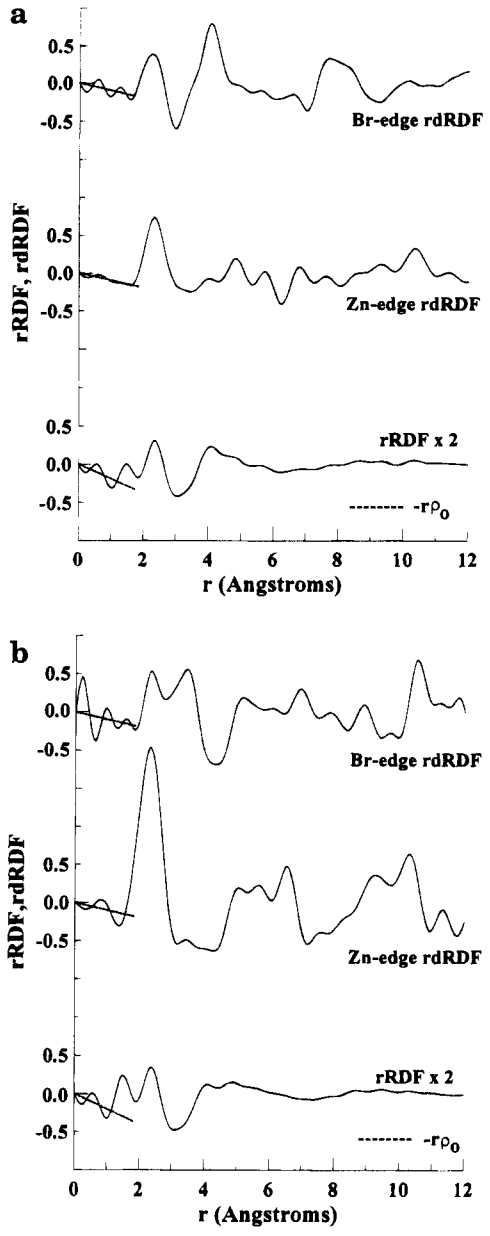

Figure 3. Reduced total and differential radial distribution functions (rRDF and rdRDF): (a) 6:1 sample; (b) 16:1 sample. In both (a) and (b) the rRDF is scaled by a factor of 2.

has a d^{10} electron configuration, there is no net energy gain from d-orbital splitting[17] and the coordination geometry therefore depends on the ligands. With large anions such as Br^-, Zn favors a tetrahedral over a square-planar geometry.[53] Support for the tetrahedral geometry comes from the Br−Br coordination at 4.05 Å, which is close to the intratetrahedral distance predicted from the Zn−Br distance:

$$R_{Br-Br} = R_{Zn-Br}(8/3)^{0.5} = 3.91 \text{ Å}$$

The complexation of the Zn in the polymer electrolyte is of the form $ZnBr_y(O)_{4-y}^{(2-y)}$, where (O) represents an oxygen from a PPO segment. In aqueous solutions of $ZnBr_2$, Raman spectroscopy has been used to identify the species $ZnBr_4^{2-}$, $ZnBr_3^-$, and $ZnBr_2$.[54-56] $ZnBr^+$ was only observed in the presence of an excess Zn^{2+},[56] so we do not expect any $ZnBr^+$ in our samples. In the aqueous solutions, the proportions of the complexes where y was 4, 3, and 2 were 3:4:2, respectively. Such a proportion ratio provides an average aqueous Br−Br coordination number just over 2. In our 6:1 sample, the Br−Br coordination is close to 5, and the EXAFS analysis does not suggest a Br−O correlation, which there would be for y equal to 2 or 3. Thus in contrast to the aqueous solution case, our results support the presence of mainly $ZnBr_4^{2-}$ and $Zn(O)_4^{2+}$.

The large Br−Br coordination may also be indicative of the formation of polybromide ions, much like the polyiodide anions studied in other polymer electrolytes.[57] However, this phenomenon only occurs in the presence of I_2 in the solution. While an interesting idea, there is no excess of Br atoms to create the polybromide anions while still maintaining overall charge neutrality.

Initially we were concerned that using PPO terminated with hydroxyl groups would affect the oxygen coordinations. The hydroxyl groups, which are better Lewis bases than the ether oxygens, will preferentially coordinate to the cations. However, for a 6:1 concentration in PPO of M_w = 4000 there are only 0.174 OH groups for *each* Zn atom present in the sample. Since $n_{Zn-O} \approx 2$, a maximum of 8.7% of the oxygens coordinating with Zn cations can come from hydroxyl groups. It is therefore unlikely that the hydroxyl groups dominated the coordination with the cations and affected the final coordination numbers. In the 16:1 sample, almost 23% of the Zn−O coordinations could come from oxygens in hydroxyl groups. The effect, if any, in the 16:1 sample could not be detected (section V.B.).

We should also mention another dissimilarity between the $[PPO]_nZnBr_2$ and aqueous $ZnBr_2$, in which the aqueous $ZnBr_2$ is proposed to form crystal-like clusters of connected $ZnBr_4^{2-}$ tetrahedra.[17,58] In our 6:1 sample, the coordination number for Br−Zn is approximately 1 and would be larger (~2) for an extended structure. Furthermore, no Zn−Zn coordination is observed in our results; an extended structure would display such a correlation at about 4 Å. This point demonstrates the usefulness of the DAS method. Without the ability to examine coordination beyond the nearest neighbors, any extended structure is easily proved or refuted.

B. $[PPO]_{16}ZnBr_2$ (16:1). Because of the poor signal-to-noise ratios in the 16:1 dSFs, we are reluctant to interpret coordination numbers determined from the dRDF. If we compare the k-space data in the 6:1 and 16:1 samples, we see from Figures 5a and 6a that the Zn EXAFS and the Zn dSFs from the 6:1 and 16:1 complexes appear quite similar within the experimental noise. This strongly suggests that the chemical and stoichiometric environment around the Zn is similar in both samples. While the Br EXAFS for the 6:1 and 16:1 complexes show a great similarity (Figure 5b), the Br dSFs (Figure 6b) are substantially different. We attribute this difference to using a scattering energy at only 6 eV below the Br edge for the 16:1 sample. The estimated incident beam bandwidth of 9.6 eV overlapped with the energies above the Br edge and introduced a nonzero $\Delta f''$ term in eq 15. This perhaps accounts for the less oscillatory nature of the 16:1 Br dSF.

Based on this k-space comparison, we cautiously suggest that the dissociated state of the $ZnBr_2$ in the 16:1 sample is similar to that in the 6:1 sample with $ZnBr_y(O)_{4-y}$, where most of the species are $ZnBr_4^{2-}$ and $Zn(O)_4^{2+}$. A constant coordination for varying salt concentration has also been suggested by EXAFS in the similar system $[PEO]_nZnX_2$[15] where X = I, Br.

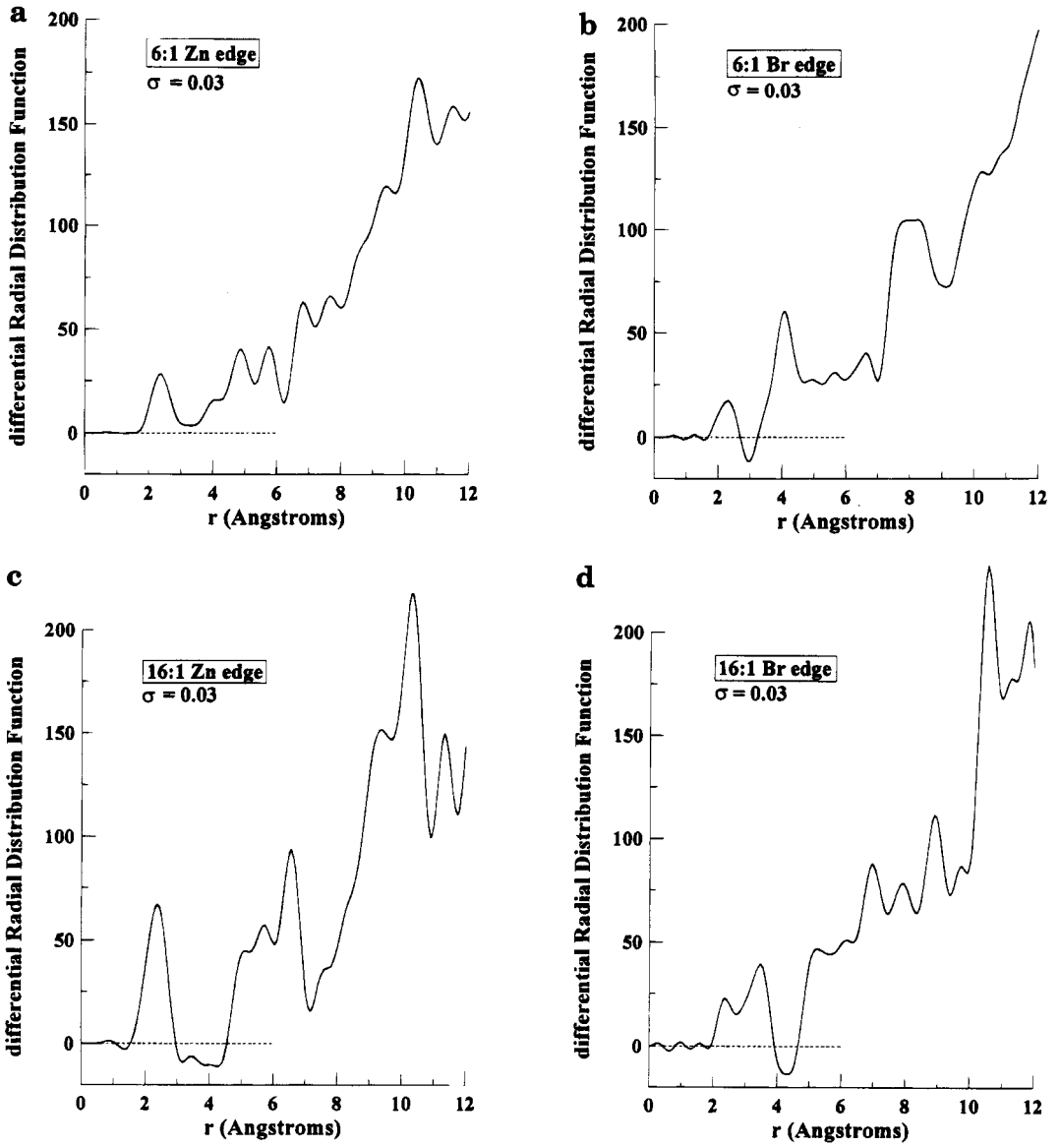

Figure 4. Differential radial distribution functions (dRDFs) from which the coordination numbers were calculated: (a) 6:1 Zn edge; (b) 6:1 Br edge; (c) 16:1 Zn edge; (d) 16:1 Br edge.

VI. Conclusions

Using a combination of EXAFS and DAS, we have identified the ionic species in the $[PPO]_nZnBr_2$ polymer electrolyte to be $ZnBr_y(O)_{4-y}$, consisting mainly of $ZnBr_4^{2-}$ and $Zn(O)_4^{2+}$, where the oxygens are part of one or more of the PPO chains. We stress that EXAFS alone cannot provide the detail revealed in the anomalous scattering experiments, yet EXAFS is an important complement in identifying the species at different distances from the central atom. The predominant ionic species are different than for $ZnBr_2$ in aqueous solutions, and this is obviously related to the Lewis base strength of the ether oxygens and the ability for the PPO chains to configure around Zn^{2+} cations in a fashion similar to crown ethers.[59]

The ionic structure revealed by our experiments is not obvious by other methods and suggests that work of this type must be performed to identify the mobile ionic species in polymer electrolytes. In cases where one or both ions contain heavy atoms with absorption edges above 8 keV, DAS experiments are appropriate; at lower scattering energies, the radial distribution analysis becomes suspect due to truncation effects. In systems containing lighter metal ions, the combination of EXAFS with neutron scattering may be more suitable, assuming that one can isotopically label the ionic species.

The coordinations found here are not very encouraging for the engineering of polymer electrolytes with high ionic conductivity. Because the cation is closely bound to the polymer chain, we imagine that the anion is the more mobile species in this complex. Meanwhile, the bulkiness and large mass of the $ZnBr_4^{2-}$ makes it a poor choice for rapid transport.

In closely related work, we have modeled DAS experiments using hard sphere structure factors in order to (1) evaluate the validity of the k-averaging used in eq 15 and (2) explore regularization and maximum entropy methods for data inversion.

In the near future, we plan to refine the structures determined in this work as well as extend this method to (1) selected ionomers containing heavy ions[60] and (2) Br-containing ionene polyelectrolytes which have been reported to undergo counterion condensation in solution.[61]

Acknowledgment. We are grateful for the support of this project through the CUMIRP program at the University of Massachusetts and the Petroleum Re-

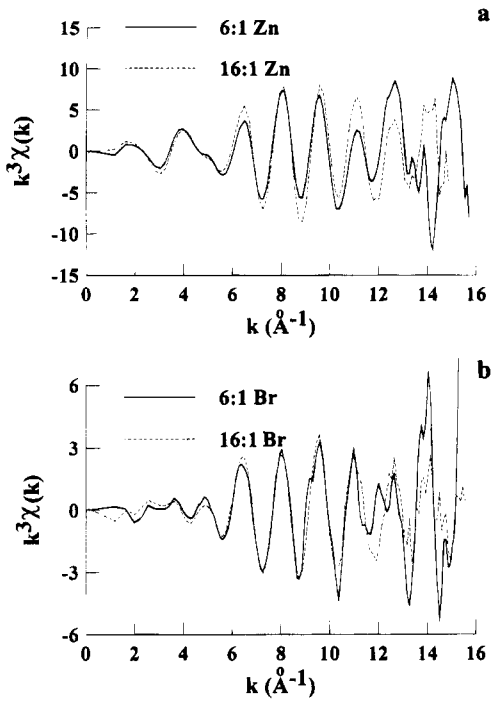

Figure 5. Comparison of the reduced EXAFS curves between the 6:1 (solid) and 16:1 (dashed) samples: (a) Zn edge; (b) Br edge.

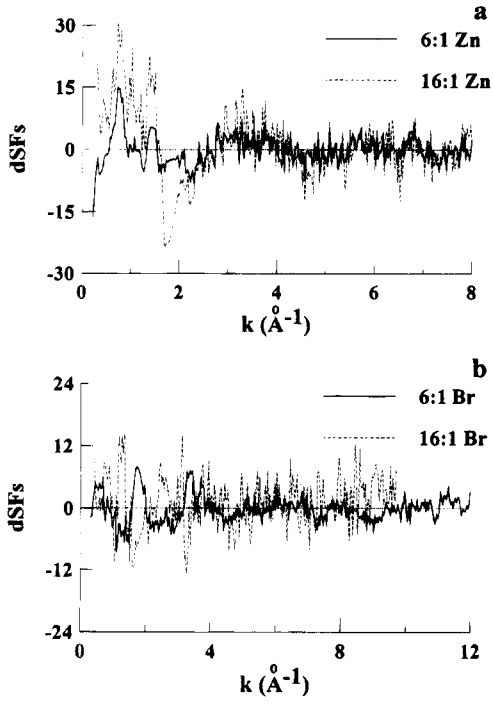

Figure 6. Comparison of the differential structure factors between the 6:1 (solid) and 16:1 (dashed) samples: (a) Zn edge; (b) Br edge.

search Fund (25856-G7P). We wish to thank W. P. Wang, M. Davis, and X. Zou for their help with the data collection, and we deeply appreciate the help and organization of the dedicated staff at the Cornell High Energy Synchrotron Source (CHESS).

References and Notes

(1) Yang, H.; Farrington, G. C. *J. Polym. Sci., Polym. Phys.* **1993**, *31*, 157.
(2) Cowie, J. M. G.; Cree, S. H. *Annu. Rev. Phys. Chem.* **1989**, *40*, 85.
(3) Wright, P. V. *Br. Polym. J.* **1975**, *7*, 319.
(4) Fenton, D. E.; Parker, J. M.; Wright, P. V. *Polymer* **1973**, *14*, 589.
(5) Farrington, G. C.; Linford, R. G. In *Polymer Electrolyte Reviews, 2*; MacCallum, J. R., Vincent, C. A., Eds.; Elsevier Applied Science: New York, 1989; p 255.
(6) Zahurak, S. M.; Kaplan, M. L.; Rietman, E. A.; Murphy, D. W.; Cava, R. J. *Macromolecules* **1988**, *21*, 654.
(7) Armand, M. B. *Annu. Rev. Mater. Sci.* **1986**, *16*, 245.
(8) Payne, D. R.; Wright, P. V. *Polymer* **1982**, *23*, 690.
(9) Armand, M. *Solid State Ionics* **1983**, *9–10*, 745.
(10) Ratner, M. A. In *Polymer Electrolyte Reviews, 1*; MacCallum, J. R., Vincent, C. A., Eds.; Elsevier Applied Science: London, 1987; Chapter 7.
(11) Druger, S. D.; Nitzan, A.; Ratner, M. A. *J. Chem. Phys.* **1983**, *77*, 3133.
(12) Teo, B. K. *EXAFS: Basic Principles and Data Analysis*; Springer-Verlag: Berlin, 1986; pp 114–157.
(13) Andrews, K. C.; Cole, M.; Latham, R. J.; Linford, R. G.; Williams, H. M. *Solid State Ionics* **1988**, *28–30*, 929.
(14) Catlow, C. R. A.; Chadwick, A. V.; Greaves, G. N.; Moroney, L. M.; Worboys, M. R. *Solid State Ionics* **1983**, *9–10*, 1107.
(15) Cole, M.; Sheldon, M. H.; Glasse, M. D.; Latham, R. J.; Linford, R. G. *Appl. Phys. A* **1989**, *49*, 249.
(16) McBreen, J.; Lin, I.-C. *J. Electrochem. Soc.* **1992**, *139*, 960.
(17) Ludwig, K. F.; Warburton, W. K.; Fontaine, A. *J. Chem. Phys.* **1987**, *87*, 620.
(18) Eisenberger, P.; Brown, G. S. *Solid State Commun.* **1979**, *29*, 481.
(19) Fuoss, P. H.; Eisenberger, P.; Warburton, W. K.; Bienenstock, A. *Phys. Rev. Lett.* **1981**, *46*, 1537.
(20) Fuoss, P. H.; Warburton, W. K.; Bienenstock, A. *J. Non-Cryst. Solids* **1980**, *35–36*, 1233.
(21) Aur, S.; Kofalt, Y.; Waseda, Y.; Egami, T.; Wang, R.; Chen, H. S.; Teo, B.-K. *Solid State Commun.* **1983**, *48*, 111.
(22) Fischer-Colbrie, A.; Bienenstock, A.; Fuoss, P. H.; Marcus, M. A. *Phys. Rev. B* **1988**, *38*, 12388.
(23) Tonnerre, J. M.; DeLima, J. C.; Raoux, D. *J. Chim. Phys.* **1989**, *86*, 1509.
(24) Ludwig, K. W., Jr.; Warburton, W. K.; Wilson, L.; Bienenstock, A. I. *J. Chem. Phys.* **1987**, *87*, 604. Ludwig, K. W., Jr.; Wilson, L.; Warburton, W. K.; Bienenstock, A. I. *J. Chem. Phys.* **1987**, *87*, 613.
(25) Schultz, E.; Bertagnolli, H.; Frahm, R. *J. Chem. Phys.* **1990**, *92*, 667.
(26) Mager, T.; Schultz, E.; Bertagnolli, H.; Frahm, R. *Ber. Bunsen-Ges. Phys. Chem.* **1990**, *94*, 703.
(27) Mager, T.; Bertagnolli, H.; Degenhardt, D.; Frahm, R. *Mol. Phys.* **1991**, *73*, 587.
(28) Dreier, P.; Rabe, P. *Rev. Sci. Instrum.* **1986**, *57*, 214.
(29) Cai, H.; Hu, R.; Egami, T.; Farrington, G. C. *Solid State Ionics* **1991**, *52*, 333.
(30) Winokur, M., private communication.
(31) Besner, S.; Vallee, A.; Bouchard, G.; Prud'homme, J. *Macromolecules* **1992**, *25*, 6480.
(32) Yang, H.; Farrington, G. C. *J. Electrochem. Soc.* **1992**, *139*, 1646.
(33) Huq, R.; Chiodelli, G.; Ferloni, P.; Magistris, A.; Farrington, G. C. *J. Electrochem. Soc.* **1987**, *134*, 364.
(34) Huq, R.; Farrington, G. C. *Solid State Ionics* **1988**, *28–30*, 990.
(35) Faber, T. E.; Ziman, J. M. *Philos. Mag.* **1965**, *11*, 153.
(36) James, R. W. *The Optical Principles of the Diffraction of X-Rays*; Oxbow Press: Woodbridge, CT, 1982; pp 135–192.
(37) Cromer, D. T.; Mann, J. B. *Acta Crystallogr.* **1968**, *A24*, 321.
(38) Kawamura, T.; Fukamachi, T. *Jpn. J. Appl. Phys.* **1978**, *Suppl. 17–2*, 224.
(39) Fishburn, J.; Barton, S. W. *Acta Crystallogr. A*, submitted for publication.
(40) Perrin, D. D.; Armarego, W. L. F. *Purification of Laboratory Chemicals*, 3rd ed.; Pergamon Press: Oxford, 1988; p 217.
(41) Eisenberger, P.; Platzman, P. M.; Winick, H. *Phys. Rev. Lett.* **1976**, *36*, 623.
(42) Sparks, C. J., Jr. *Phys. Rev. Lett.* **1974**, *33*, 262.
(43) McMaster, W. H.; Kerr del Grande, N.; Mallett, J. H.; Hubbell, J. H. UCRL-50174 Sec. II, Rev. I, 1969.
(44) Hoyt, J. J.; deFontaine, D.; Warburton, W. K. *J. Appl. Crystallogr.* **1984**, *17*, 344.
(45) Aur, S.; Kofalt, D.; Waseda, Y.; Egami, T.; Chen, H. S.; Teo, B. K.; Wang, R. *Nucl. Instrum. Methods Phys. Res.* **1984**, *222*, 259.
(46) Waseda, Y. *The Structure of Non-Crystalline Materials*; McGraw-Hill, Inc.: New York, 1980; pp 27–51.
(47) Krogh-Moe, J. *Acta Crystallogr.* **1956**, *9*, 951.
(48) Norman, N. *Acta Crystallogr.* **1957**, *10*, 370.

(49) Malet, G.; Cabos, C.; Escande, A.; Delord, P. *J. Appl. Crystallogr.* **1973**, *6*, 139.
(50) Hadju, F. *Acta Crystallogr.* **1972**, *A28*, 250.
(51) Waser, J.; Schomaker, V. *Rev. Mod. Phys.* **1953**, *25*, 671.
(52) Goggin, P. L.; Johansson, G.; Maeda, M.; Wakita, H. *Acta Chem. Scand.* **1984**, *A38*, 625.
(53) Huheey, J. E. *Inorganic Chemistry: Principles of Structure and Reactivity*, 2nd ed.; Harper and Row: New York, 1978; pp 429–430.
(54) Yellin, W.; Plane, R. A. *J. Am. Chem. Soc.* **1961**, *83*, 2448.
(55) Kanno, H.; Hirashi, J. *J. Raman Spectrosc.* **1980**, *9*, 85.
(56) Yang, M. M.; Crerar, D. A.; Irish, D. E. *J. Solution Chem.* **1988**, *17*, 751.
(57) Hardy, L. C.; Shriver, D. F. *J. Am. Chem. Soc.* **1986**, *108*, 2887. Lerner, M. M.; Lyons, L. J.; Tonge, J. S.; Shriver, D. F. *Chem. Mater.* **1989**, *1*, 601. zur Loye, H.-C.; Heyen, B. J.; Marcy, H. O.; DeGroot, D. C.; Kannewurf, C. R.; Shriver, D. F. *Chem. Mater.* **1990**, *2*, 603. Lerner, M. M.; Tipton, A. L.; Shriver, D. F.; Dembek, A. A.; Allcock, H. R. *Chem. Mater.* **1991**, *3*, 1117.
(58) Largarde, P.; Fontaine, A.; Raoux, D.; Sadoc, A.; Migliardo, P. *J. Chem. Phys.* **1980**, *72*, 3061.
(59) Weber, E.; Toner, J. L.; Goldberg, I.; Vögtle, F.; Laidler, D. A.; Stoddard, J. F.; Bartsch, R. A.; Liotta, C. L. *Crown Ethers and Analogs*; John Wiley & Sons: New York, 1989.
(60) Vlaic, G. In *Structure and Properties of Ionomers*; Pineri, M., Eisenberg, A., Eds.; D. Riedel Publishing Co.: Dordrecht, Holland, 1987; pp 51–72. Ding, Y. S.; Cooper, S. L. In *Structure and Properties of Ionomers*; Pineri, M., Eisenberg, A., Eds.; D. Riedel Publishing Co.: Dordrecht, Holland, 1987; pp 73–86.
(61) Klein, J. W.; Ware, B. R. *J. Chem. Phys.* **1983**, *80*, 1334.

MA941291X